2013-06

High-sensitivity optical humidity sensor based on a thin dielectric waveguide

Applied Optics,Washington, DC : Optical Society of America - OSA,v. 52, n. 18, p. 4287-4293 , June 2013

http://www.producao.usp.br/handle/BDPI/45284

High-sensitivity optical humidity sensor based on a thin dielectric waveguide

R. A. S. Ribeiro, J. F. M. Domenegueti, and S. C. Zilio*

Instituto de Física de São Carlos, Universidade de São Paulo, Caixa Postal 369, 13560-970, São Carlos, SP, Brazil

*Corresponding author: zilio@ifsc.usp.br

Received 22 February 2013; revised 25 April 2013; accepted 20 May 2013; posted 21 May 2013 (Doc. ID 185805); published 18 June 2013

A low-cost, high-sensitivity humidity sensor based on a low-loss dielectric thin film waveguide (WG) is presented. The guided mode is produced by coupling laser light into the film by optical tunneling through a solid gap deposited on the base of a semi-cylindrical lens. The light reflected from this optical system carries information about the refractive index of the medium neighboring the WG, and is detected by a low-cost CCD linear sensor and analyzed with a microcontroller or personal computer. The technique presents good sensitivity to relative humidity (RH) changes, especially below 10% RH, linear behavior between 20% and 80% RH, and a response time of a few seconds. © 2013 Optical Society of America

OCIS codes: (120.0280) Remote sensing and sensors; (310.2785) Guided wave applications.
http://dx.doi.org/10.1364/AO.52.004287

1. Introduction

The accurate measurement and control of humidity is important for a variety of applications. This motivates the development of new techniques and devices aiming at improving humidity sensors [1,2]. Such improvements should tackle important issues related to reliability, cost, sensitivity, accuracy, and response time. Humidity sensors usually rely on the change of some physical parameter of a humidity-sensing material, generally shaped in the form of a thin film. A number of techniques to probe the properties of these films and to get better response times have recently been reported. Most of them measure variations of a given parameter that can be of electrical [3,4], acoustical [5,6], or optical [7–9] nature. In principle, optical sensors can be more advantageous than their electrical counterpart as they are less sensitive to electromagnetic interference. Particularly, optical methods based on evanescent waves (EW) were shown to be useful to probe the effects of relative humidity (RH) in thin films deposited on silica [10–13] and plastic [14] optical fibers. Planar waveguides (WGs) also constitute good tools to generate a probe EW and are employed in techniques using surface plasmon resonance (SPR) [15] and dielectric thin films WGs [16], which are versatile and accurate devices for refractive index (RI) measurements. Since the EW penetrates a fraction of the wavelength into the medium surrounding the WG, it probes both the adsorbed layer (of a few angstroms) as well as the outer gas layer. It is important to note that in order to use the SP WG as a humidity sensor, it is necessary to coat the device with a transducing layer whose RI is humidity dependent. In the case of dielectric WGs, the WG material itself is hydrophilic, and this behavior avoids any extra humidity-dependent layers. This is interesting because the humidity-sensing film can age, and its performance may be degraded if a long-lasting operation is desired.

A mode propagating in a planar dielectric WG exhibits interference for light traveling perpendicular to the WG, resulting in a standing wave in that direction. From this point-of-view, the dielectric thin film can be regarded as a Fabry–Pérot (FP) étalon [17].

1559-128X/13/184287-07$15.00/0

Therefore, methods based on WGs have the intrinsic sensitivity of interferometric techniques but are much more compact than usual interferometers. Large amounts of light can be efficiently coupled into a planar WG by means of a prism coupler [18–20], as done in the *m*-line technique, which widely used for the characterization of thin films [21,22]. As the EW associated with the guided mode interacts with the nearby medium, any change in its RI has a major influence on the propagation conditions of the WG. Since the coupled light reflects back to the prism coupler after propagating a small distance along the WG, the analysis of this reflected light provides information about changes in the sample RI. For the *m*-line technique, the high-index WG is deposited on top of a lower-index substrate, which is pushed against a high-index prism, usually made of rutile. Although this procedure enables control of the air gap thickness, and thus the coupling efficiency, it is quite sensitive to the surface flatness and to any dirt between the two surfaces. Besides, the sample to be measured has to flow through the gap, which is on order of the WG.

The present work studied a low-loss dielectric thin film WG device for the measurement of RH. Although optical fiber WGs coated with humidity-sensing thin films were already used in RH measurements, the present sensor is the first that employs a planar WG without using an extra humidity-sensing film. This configuration yields a high sensitivity to low RH values, in contrast to the vast majority of sensors presented in the literature, whose sensitivity has an exponential type behavior at low RH values. The device consists of two dielectric layers deposited on the base of a high RI semi-cylindrical glass lens (coupler), which acts as a focusing lens, providing simultaneous access to many different incident angles. The high RI WG layer has its outer surface in contact with the sample to be measured and is separated from the coupler by a low RI layer. This buffer layer produces an EW that leaks into the WG via optical tunneling, and its thickness defines how much light is coupled into the WG. The basic principle responsible for the RH sensing is the dependence of the coupling angle on the humidity. This angle can be determined by a simple inspection of the light pattern reflected by the system. The sensor has no moving parts, and it is rugged, inexpensive, user-friendly, and compact. The device was applied to the measurement of RH, presenting a good sensitivity level and fast response time. The advantage of this technique over the usual *m*-line setup is the replacement of the air gap by a solid layer that avoids the problem of dirt between the two surfaces and allows an easier gas flow. This circumvents the need of tuning the air gap to optimize the coupling to the WG. When compared to the SPR sensor [15], the dielectric WG circumvents the use of an extra humidity-sensing film, making the sensor more reliable. Since it is made with a low-loss material, it presents resonance lines that are sharper than the plasmon resonance lines, which makes the device more accurate.

2. Experiment

In the setup shown in Fig. 1(a), a semi-cylindrical coupler lens replaces the equilateral prism employed in the *m*-line technique, saving one focusing lens and making the system more compact. Regardless of how well the incoming beam is collimated, the semi-cylindrical lens automatically gives simultaneous access to many different angles incident on the prism base. This geometry, recently used to measure the critical angle in internal reflection [23], produces a lateral magnification of the laser beam, which is a positive feature of the setup because it increases the sensitivity. The semi-cylindrical coupler has a typical radius on the order of 10 mm, and is made of flint glass with an RI around 1.7. The first layer evaporated on the coupler has a low RI and produces an EW that leaks into the high-index WG layer via optical tunneling. It plays the role of the input coupler in a FP étalon, defining the input transmittance. Increasing the layer thickness amounts to decreasing the coupling coefficient exponentially. The second layer is the high-index WG corresponding to the étalon itself, with the surface in contact with the sample working as a mirror with unit reflectivity. Thus, we have a WG separated from the prism by a solid dielectric gap in contrast to the usual prism coupler

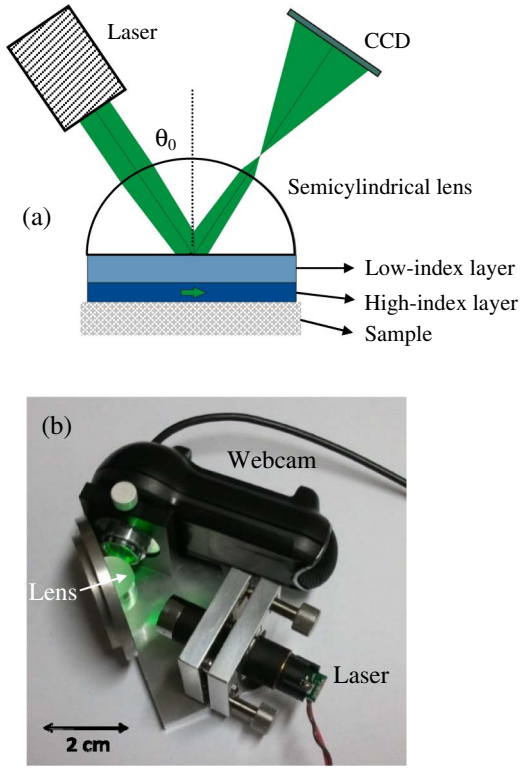

Fig. 1. (a) Diagram showing the semi-cylindrical coupler, the low-index coupling layer, the WG layer, and the sample. (b) Optical setup using a 532 nm laser pointer and web camera.

where an air gap separates them. A similar arrangement, with an equilateral prism, was already used as an atomic mirror, owing to the large electric field enhancement [17]. The build-up of the electric field inside the WG is determined by the coupling coefficient and the losses. The optimum is reached when the coupling matches the losses in the cavity; the smaller the losses, the larger the optimum buildup coefficient.

For the sake of comparison, the dielectric layers were evaporated in two ways—either by a conventional electron beam-physical vapor deposition (EB-PVD) process in a Balzers BAK600 evaporator, or by ion-beam-assisted deposition (IBAD) in a Leybold CCS Pro evaporator, with the semi-cylindrical coupler maintained at 200°C and the oxygen pressure in the chamber kept around 2×10^{-4} mbar, in both cases. During evaporation, the thicknesses were monitored with a quartz oscillator thickness gauge. An 800 nm-thick SiO_2 coupling layer ($n_{SiO2} = 1.46$) was evaporated onto the semi-cylindrical coupler base, followed by a 65 nm-thick ZrO_2 WG layer ($n_{ZrO2} = 2.06$) in the case of EB-PVD, or, in the case of IBAD, 60 nm of Dralo ($n_{Dralo} = 2.2$), which is basically TiO_2 with a given amount of Al_2O_3 added to reduce the index of refraction to enable wider AR bandwidth in eyeglasses. The target materials for evaporation were purchased from Umicore and used as received. The values of the thicknesses were initially calculated with the Essential Macleod thin film coatings software and confirmed afterward by measuring the reflectance spectrum.

As a light source, we used a low-cost 532 nm laser pointer, whose position is chosen such that the beam forms an angle that allows light to be coupled into the WG, as discussed below. This angle is about 56 deg. The laser light was *s*-polarized by a low-cost plastic linear polarizer. With the purpose of visualizing the profile of the light reflected by the coupler, we used a low-cost web camera and image software with computer. However, in order to make the system cheaper and more compact, a CCD monochrome linear sensor (Sony ILX554B) and microcontroller were employed in manufacturing of the actual sensor. The CCD is positioned symmetrically to the laser pointer, and its distance to the focal point, shown in Fig. 1(a), can be adjusted as a way to change the responsivity of the sensor by covering a different number of pixels in the CCD. As we will discuss later, the Dralo WG is less sensitive to RH variations, and the CCD is placed farther such the system has the same overall response as the one with the ZrO_2 WG. Although not essential, this is an interesting procedure because it allows the laser beam to cover more pixels of the CCD. As seen in Fig. 1(b), both the laser and CCD are fixed on a metal baseplate, and the coupler is glued perpendicularly to a steel baseplate with a central opening to allow contact with the moist air. The only moving part is the laser holder that is used to center the reflected profile in the CCD linear array. After such tuning, the assembly should not be readjusted.

The light impinges normally to the cylindrical surface to minimize astigmatism. When the incidence angle is greater than the critical angle, the light is totally reflected. However, for some angles called synchronous angles, a part of the light is coupled into the WG before being totally reflected [21]. According to Tien and Ulrich [18], these angles can be obtained when the phase matching conditions for light propagating inside in the WG are satisfied. A typical angle-dependent *m*-line profile observed in the far field is made of dips related to each mode guided by the guide. To obtain precise results, a goniometer with good accuracy is needed for the measurement of synchronous angles. On the other hand, a differential device relies only on the knowledge of angle variations and not on their absolute values. The synchronous angle is very sensitive to the parameters of the system, but if all of them are kept constant, except for the RH of the sample, it is possible to determine its variation by measuring small deviations of the synchronous angle. This allows for the development of a differential sensor, where the synchronous angle has to be calibrated against the RH prior to use.

As shown by the web camera image depicted in Fig. 2(a), oscillations appear in the reflected light profile at the Fresnel zone, as already discussed in [24]. They can be regarded as the interference between the part of the beam that is directly reflected from the coupler base and that reflected after being guided inside the high-index film. These oscillations, which are more accentuated when a low-loss WG is employed, follow the synchronous angle and can be used to probe the medium surrounding the WG.

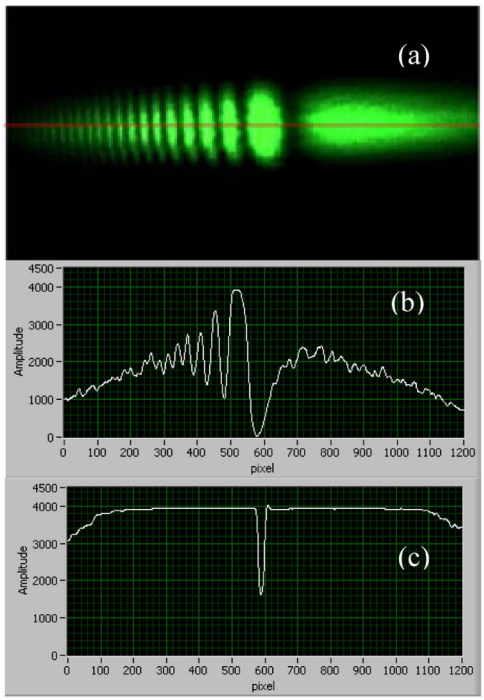

Fig. 2. (a) Image obtained with a web camera for attenuated laser power. (b) Intensity profile measured by the CCD linear array at lower and (c) higher laser powers.

As the sample conditions change, the fringe profile moves left or right. In Fig. 2(a), the laser beam was attenuated to show the real profile, but under this condition, the borders of the pattern may be irregular and introduce noise to the intensity profile. This can be seen in Fig. 2(b) where the web camera was replaced by the CCD linear array. To circumvent this problem, one can work with a higher laser power (~1 mW) to saturate the image, as in Fig. 2(c), and measure the minimum, as recently done in [23]. Therefore, the operating principle of this RH sensor relies on determining the position of the minimum of Fig. 2(c) as the humidity changes.

To verify the performance of this RH WG sensor, we used a homemade humidity chamber, kept at atmospheric pressure and constant temperature. RH within the chamber was changed by controlling the flux ratio between dry nitrogen gas and moist nitrogen gas. The moist gas was obtained by bubbling nitrogen gas inside water contained in an interconnected vessel. The RH calibration was achieved by taking the average value read with two commercial probes, with an average accuracy of about 1.5% below 90% RH, located at different positions inside the container. This setup was used to calibrate the pixel number by measuring the position of the minimum shown in Fig. 2(c) as a function of RH. However, since this humidity chamber requires a few minutes to adjust the RH, the sensor's response time was characterized by blowing moist gas directly onto the WG for one minute and then letting the system evolve to ambient RH for another minute. This procedure brings some limitation to the fastest time that can be measured, which is estimated to be of a few seconds, because the valve controlling the flux of moist gas has to be open manually.

3. Results and Discussion

Figure 3 depicts the pixel number corresponding to the position of the minimum as a function of the RH for both the ZrO_2 and Dralo WGs. In these measurements, the temperature was kept at 22°C, and the atmospheric pressure was 900 mbar. The results cover a wide range of RH, and in order to better visualize the behavior at a small RH, a logarithmic scale was used. First, we note that the positions of the minimums of the interference pattern have the same response against RH regardless if the high-index film is ZrO_2 or Dralo. This is only true because the CCD is farther from the coupler when the WG is made with Dralo, which was evaporated with the IBAD technique. In fact, as demonstrated by Martin *et al.* [25], the packing densities of SiO_2, TiO_2, and ZrO_2 films increase substantially when they are produced under ion bombardment, as measured by the reduction in the adsorption of moisture when the films are exposed to a humid atmosphere. In a ZrO_2-SiO_2 multilayer interference filter, changes in the wavelength of the peak transmittance on exposure to the atmosphere have been reduced by a factor of eight for IBAD films when compared to the conventional EB-PVD process. Therefore, IBAD films are more compact, and this reduced porosity makes them less sensitive to moisture. These facts were corroborated by structural and textural characterization, including SEM micrographs [25]. However, this difference can be circumvented by changing the position of the CCD, as described earlier, such that the response of the WG sensor does not depend significantly on the dielectric material. Actually, the sensitivity of the WG itself depends on the porosity and thickness of the WG, as observed in [4 and 25], but the response of the complete sensor can be adjusted to compensate it by changing the CCD position. With this procedure, both sensors have the same behavior, as shown in Fig. 3. The small difference between ZrO_2 and Dralo data is related to uncertainties of the commercial sensors, which are responsible for the error bars in the abscissa of Fig. 3. In addition, we found no observable hysteresis in the adsorption/desorption cycle for times on the order of a few seconds.

An interesting aspect of the responsivity plot of Fig. 3 is the fast variation of the interference minimum for RH values below 10%. We attribute this behavior to the increase in the surface coverage by water molecules when the first monolayer is formed. Attenuated total reflection (ATR) infrared spectroscopy of water adsorbed on a silicon oxide surface shows that up to three monolayers are formed when the RH reaches 30% [26], implying that the first monolayer builds up below 10% RH. These conclusions were reached by monitoring the O-H stretching vibration peak positions, which enabled us to observe ice-like water (H_2O interacting with the surface) and liquid water, as a function of humidity. To understand the origin of the rapid increase of the interference minimum for small RH values, we consider the resonance condition for the modes of the WG [18]:

$$2d_W \frac{\omega}{c} n_W \cos\theta_W = \varphi_{WS} + \varphi_{WC} + 2m\pi, \qquad (1)$$

where $m = 0, 1, 2, \ldots$ gives the order of the mode; n_W and d_W are the RI and thickness of the WG,

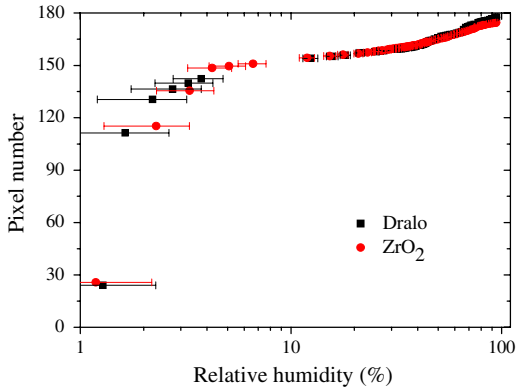

Fig. 3. Position of the minimum of the reflected profile as a function of RH for ZrO_2 (solid circles) and Dralo (solid squares) at 22°C. The error bars are given by the uncertainty of the commercial sensor.

respectively; θ_W is the angle of refraction in the WG layer; φ_{WS} and φ_{WC} are the phase changes at total internal reflection on the WG sample boundary and WG coupler layer boundary, respectively. For our system, with $d_W \sim 60$ nm, the only allowed resonance corresponds to the TE mode with $m = 0$. In addition, since φ_{WC} is constant, θ_W depends only on φ_{WS}. θ_W is related to the synchronous angle according to: $n_W \sin \theta_W = n_P \sin \theta_P$, where n_P is the RI of the semi-cylindrical coupler lens, and θ_P is the synchronous angle. Therefore, the synchronous angle depends only on the phase change of the total internal reflection at the WG sample boundary, which is expected to be much more sensitive to the formation of the first monolayer, because in this process the RI at the surface of the WG jumps from 1 to about 1.334.

Although the behavior of this WG sensor at low RH is interesting because it demonstrates the formation of the first monolayer of water molecules, measurements below 20% RH are not of practical interest. Most products manufactured and processed in cleanroom environments demand RH ranging from 35%–65%. Below 30% RH, there is very little moisture in the air to dissipate static charges, which are capable of doing physical damage to sensitive electronic parts. On the other hand, the presence of fungi for RH above 70% may become a problem. However, the WG sensor presented here also has good performance in the range of interest, as seen in Fig. 4. After the first monolayer is formed, there is an approximately homogeneous water film on top of the WG. Supposing that the water layer thickness is proportional to the RH, the thin film coatings software predicts a linear behavior for the responsivity, as shown by the solid line in Fig. 4. This feature is interesting because it simplifies the calibration of the sensor once two known values of RH are necessary. In addition, the vapor not adsorbed does not contribute significantly to the results because its RI increases only moderately with the RH [27]. However, the fact that the present sensor needs a calibration with some commercially available device limits the accuracy to that of the sensor used for the calibration procedure. In our setup, for instance, we used a device whose accuracy was about 1.5% below 90% RH, and therefore, we end up with the same accuracy. On the other hand, the sensitivity is determined by the accuracy that the pixel corresponding to the minimum of Fig. 2(d) is found. If LabVIEW software is used, its peak-detector VI can provide an accuracy of 0.1 for the pixel position. On the other hand, if a microcontroller is employed, the centroid method [28] also provides the same type of accuracy. An analysis of Figs. 3 and 4 leads to the following conclusions. In the range 20%–80% RH (Fig. 4), the total peak variation is about 17, meaning 3.5% RH per pixel, which results in a sensitivity of 0.35% RH. In the range of smaller RH values, the sensitivity is better than 0.1% RH, as seen in Fig. 3.

As we mentioned earlier, the synchronous angle, or alternatively, the position of the minimum of the interference pattern, has to be calibrated for the RH, which can be done by considering just two points in measurements, as those depicted in Fig. 4. The calibration is carried out just once since the position of the CCD is fixed for the subsequent measurements. Using this fixed geometry and the procedure described in Section 2, we characterized the response times of both sensors. The results, shown in Fig. 5, indicate a good reproducibility. The maximum values of the square-like curve for the ZrO_2 WG are constant because of the well-defined RH of moist gas. However, we observe some fluctuations in the lower part

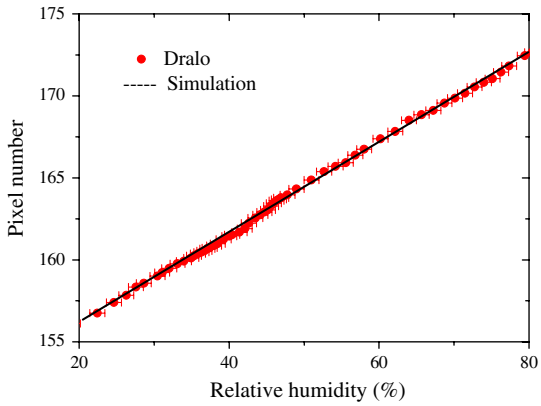

Fig. 4. Position of the minimum of the reflected profile as a function of RH for and Dralo at 22°C. The error bars are given by the uncertainty of the commercial sensor. The solid line represents a simulation carried out with the Essential Macleod thin film coatings software, assuming that the water layer thickness is proportional to the RH.

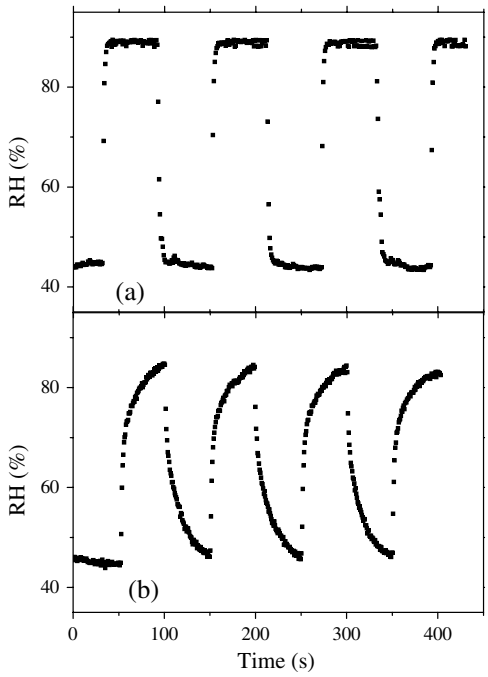

Fig. 5. Transient response curve for (a) ZrO_2 and (b) Dralo WGs between 45% and 90% RH.

of the curve because, in this case, the humidity is defined by the ambient, which can fluctuate along the measurement. We found that the 90% response and 45% recovery times were about 2 and 3 s, respectively, for the ZrO_2 WG. The actual times are expected to be shorter because, as we mentioned earlier, the valve that controls the moist gas flux is operated manually. On the other hand, the Dralo WG has long response (~15 s) and recovery (~18s) times. It is known that the response time of dielectric films are dependent on their morphology and porosity [3,4]. The ZrO_2 WG was evaporated by EB-PVD and is more porous than the Dralo WG, which was evaporated by IBAD [25]. According to [4] and [7], the increase in porosity amounts to decreasing the response time, which is in agreement with our findings. Because the films we used are fairly compact, we measured response times that are one order-of-magnitude longer than those recently reported for state-of-art sensors (see Table in [3]), even for our fast ZrO_2 WG sensor. However, it is possible that the times obtained could be significantly faster if nanostructured films achieved by glancing angle deposition were used during the evaporation of the WG. However, in this case, the performance of the sensor has to be tested against losses that may arise owing to the fairly large optical scattering that such films produce.

4. Conclusions

Optical humidity sensors based on planar dielectric WGs were fabricated. They were shown to have a high sensitivity, especially in the region of low RH, where the vast majority of sensors are not efficient. We have explained this behavior by assuming that the enhanced sensitivity at lower RH values is related to the surface coverage factor as the first monolayer is building up. For RH above 30%, the sensor presents a linear response without any observable hysteresis in the time scale of a few seconds. We obtained a sensitivity of 0.35% RH in the range 20%–80% RH, and an even better value in the range of smaller RH. The accuracy of the device is limited by the accuracy of the commercial sensor used for calibration. Furthermore, we have used this sensor for over one year without any performance degradation, as one should expect from a compactly evaporated thin film.

Regarding the response time of a few seconds, although this can be considered as a fast detector, this time could be shortened if nanostructured films were evaporated with the glancing angle deposition technique. However, tests have to be carried out in order to verify is optical scattering will be deleterious to the sensor's performance.

The present study was supported by Fundação de Amparo à Pesquisa do Estado de São Paulo (FAPESP) and Conselho Nacional de Desenvolvimento Científico e Tecnológico (CNPq).

References

1. Z. Chen and C. Lu, "Humidity sensors: a review of materials and mechanisms," Sens. Lett. **3**, 274–295 (2005).
2. C.-Y. Lee, "Humidity sensors: a review," Sens. Lett. **3**, 1–15 (2005).
3. H. Y. Wang, Y. Q. Wang, Q. F. Hua, and X. J. Li, "Capacitive humidity sensing properties of SiC nanowires grown on silicon nanoporous pillar array," Sens. Actuators B **166–167**, 451–456 (2012).
4. J. J. Steele, M. T. Taschuk, and M. J. Brett, "Response time of nanostructured relative humidity sensors," Sens. Actuators B **140**, 610–615 (2009).
5. A. Buvailo, Y. Xing, J. Hines, and E. Borguet, "Thin polymer film based rapid surface acoustic wave humidity sensors," Sens. Actuators B **156**, 444–449 (2011).
6. Y. Li, C. Deng, and M. Yang, "A novel surface acoustic wave-impedance humidity sensor based on the composite of polyaniline and poly(vinyl alcohol) with a capability of detecting low humidity," Sens. Actuators B **165**, 7–12 (2012).
7. Y. J. Liu, J. Shi, F. Zhang, H. Liang, J. Xu, A. Lakhtakia, S. J. Fonash, and T. J. Huang, "High-speed optical humidity sensors based on chiral sculptured thin films," Sens. Actuators B **156**, 593–598 (2011).
8. L. H. Chen, T. Li, C. C. Chana, R. Menon, P. Balamurali, M. Shaillender, B. Neu, X. M. Ang, P. Zu, W. C. Wong, and K. C. Leong, "Chitosan based fiber-optic Fabry–Perot humidity sensor," Sens. Actuators B **169**, 167–172 (2012).
9. B. C. Yadav, N. Verma, and S. Singh, "Nanocrystalline SnO_2-TiO_2 thin film deposited on base of equilateral prism as an opto-electronic humidity sensor," Opt. Laser Technol. **44**, 1681–1688 (2012).
10. A. Alvarez-Herrero, H. Guerrero, E. Bernabeu, and D. Levy, "Analysis of nanostructured porous films by measurement of adsorption isotherms with optical fiber and ellipsometry," Appl. Opt. **41**, 6692–6701 (2002).
11. A. Alvarez-Herrero, H. Guerrero, and D. Levy, "High-sensitivity sensor of low relative humidity based on overlay on side-polished fibers," IEEE Sens. **4**, 52–56 (2004).
12. A. Gaston, I. Lozano, F. Perez, F. Auza, and J. Sevilla, "Evanescent wave optical-fiber sensing (temperature, relative humidity, and pH sensors)," IEEE Sens. **3**, 806–811 (2003).
13. L. Xu, J. C. Fanguy, K. Soni, and S. Tao, "Optical fiber humidity sensor based on evanescent-wave scattering," Opt. Lett. **29**, 1191–1193 (2004).
14. S. K. Khijwania, K. L. Srinivasan, and J. P. Singh, "An evanescent-wave optical fiber relative humidity sensor with enhanced sensitivity," Sens. Actuators B **104**, 217–222 (2005).
15. M. N. Weiss, R. Srivastava, and H. Groger, "Experimental investigation of a surface plasmon-based integrated-optic humidity sensor," Electron. Lett. **32**, 842–843 (1996).
16. F. R. Flory, ed., *Thin Films for Optical System* (CRC Press, 1995).
17. R. Kaiser, Y. Lévy, N. Vansteenkiste, A. Aspect, W. Seifert, D. Leipold, and J. Mlynek, "Resonant enhancement of evanescent waves with a thin dielectric waveguide," Opt. Commun. **104**, 234–240 (1994).
18. P. K. Tien and R. Ulrich, "Theory of prism-film coupler and thin-film light guides," J. Opt. Soc. Am. **60**, 1325–1337 (1970).
19. R. Ulrich, "Theory of prism-film coupler by plane wave analysis," J. Opt. Soc. Am. **60**, 1337–1350 (1970).
20. P. K. Tien, "Light waves in thin films and integrated optics," Appl. Opt. **10**, 2395–2412 (1971).
21. Y. Levy, "Étude du champ inhomogène obtenu par la réflexion totale d'une onde plane sur un système de couches minces," Nouv. Rev. d'Optique Appliquée **3**, 25–30 (1972).
22. J. Cardin and D. Leduc, "Determination of refractive index, thickness and the optical losses of thin films from prism-film coupling measurements," Appl. Opt. **47**, 894–900 (2008).
23. S. C. Zilio, "A simple method to measure critical angles for high-sensitivity differential refractometry," Opt. Express **20**, 1862–1867 (2012).
24. S. Monneret, P. Huguet-Chantôme, and F. Flory, "*m*-lines technique: prism coupling measurement and discussion of

accuracy for homogeneous waveguides," J. Opt. A **2**, 188–195 (2000).
25. P. J. Martin, H. A. Macleod, R. P. Netterfield, C. G. Pacey, and W. G. Sainty, "Ion-beam-assisted deposition of thin films," Appl. Opt. **22**, 178–184 (1983).
26. D. B. Asay and S. H. Kim, "Evolution of the adsorbed water layer structure on silicon oxide at room temperature," J. Phys. Chem. B **109**, 16760–16763 (2005).
27. "Manufacturing Engineering Laboratory—Engineering Metrology Toolbox," National Institute of Standard Technology, 28 Dec. 2011, http://emtoolbox.nist.gov/Main/Main.asp.
28. W. Ecke, A. A. Chertoriiski, and V. L. Vesnin, "A high-speed system for strain and temperature measurements based on fiber Bragg sensors," Instrum. Exp. Tech. **50**, 565 (2007).